Journal of Zhejiang University-SCIENCE B (Biomedicine & Biotechnology) in press
www.jzus.zju.edu.cn; www.springer.com/journal/11585
E-mail: jzus_b@zju.edu.cn

Research Article

https://doi.org/10.1631/jzus.B2500767

Selenocystine-based fluorescence assay combined with structural prediction for functional analysis of cystine transporter variants in cystinuria

Xiaobai HE[1], Xinyi QIAN[1], Xiaoguang ZHENG[1], Hong ZHANG[1], Jinbang SHAO[1], Xiaopan CHEN[2], Qi RUAN[1], Jianxin LYU[1,3]✉, Leixiang YANG[2]✉, Linjie CHEN[1]✉

[1]*School of Laboratory Medicine and Bioengineering, Zhejiang Provincial People's Hospital, Hangzhou Medical College, Hangzhou, 311399, China*

[2]*Department of Genetic and Genomic Medicine, Zhejiang Provincial People's Hospital, Affiliated People's Hospital, Hangzhou Medical College, Hangzhou, 310014, China*

[3]*Zhejiang Provincial Engineering Research Centre for Key Technology of Diagnostic Testing, Hangzhou, 310053, China*

Abstract: Objective: Cystine stones account for 1%–2% of adult and up to 10% of pediatric kidney stones. They result from cystinuria, an autosomal recessive disorder caused by mutations in solute carrier family 3 member 1 (SLC3A1) and solute carrier family 7 member 9 (SLC7A9), which encode the renal cystine transporter subunits. These mutations impair cystine reabsorption, raising urinary cystine levels and driving stone formation. Current diagnostic options remain limited in terms of detecting molecular-level dysfunctions. Thus, we aimed to develop a nonradioactive, cell-based method for the functional assessment of cystine transporters and mutation-specific pathologies. Methods: Using HEK293 cells transiently co-expressing wild-type or mutant SLC3A1 and SLC7A9, we developed an integrated approach that combines a selenocystine-based fluorescence uptake assay with AlphaFold3-based structural predictions to rapidly and accurately assess cystine transporter function and the molecular impact of genetic mutations. Results: The affinity of the SLC3A1/SLC7A9 complex was comparably apparent for selenocystine (Km=(156.3±24.2) μmol/L) and cystine (literature Km about 200 μmol/L). Using operational thresholds (mild >60%, moderate 20%–60%, severe <20% residual activity), the assay differentiated the functional impact of eight clinically characterized variants, including SLC7A9 A70V, A182T, G105R, R333W, V170M, A354T, and P482L, and SLC3A1 M467T, with categorical assignments consistent with previously published radioisotope-based functional data. AlphaFold3 modelling, combined with molecular docking, provides mechanistic interpretations

✉ Linjie CHEN, chenlinjie@hmc.edu.cn;
Leixiang YANG, yangleixiang@hmc.edu.cn;
Jianxin LYU, jxlu313@163.com.
Xiaobai HE, http://orcid.org/0000-0009-9485-5265
Jianxin LYU, http://orcid.org/0000-0003-2343-1666
Leixiang YANG, http://orcid.org/0000-0001-9020-7336
Linjie CHEN, http://orcid.org/0009-0007-7431-4490

Received Nov. 25, 2025; Revision accepted May 13 2026;
Crosschecked xxx. xx, 20xx; Published online xxx. xx, 20xx

of the dysfunction observed in the P482L and A354T mutants. Conclusions: The integrated approach employed in this work, which combines a sensitive selenocystine fluorescence assay with AI-powered structural analysis, enables the rapid, precise diagnosis of cystinuria variants. This platform is compatible with standard microplate-reader infrastructure and offers potential utility in variant-interpretation pipelines and future genotype-guided therapeutic decision-making, pending prospective clinical validation.

Key words: Cystinuria; SLC3A1; SLC7A9; Selenocystine; Diagnosis; Mutation

1 Introduction

Cystine stones, that account for 1%–2% of adult kidney stones and up to 10% in pediatric patients, result from cystinuria, an autosomal recessive disorder caused by mutations in the solute carrier family 3 member 1 (SLC3A1) and solute carrier family 7 member 9 (SLC7A9) genes. These mutations impair renal cystine reabsorption, promoting crystallization (Chillaron et al., 2010; Copelovitch, 2012; Thomas et al., 2014; Servais et al., 2021). Therefore, early diagnosis and targeted intervention are critical to prevent the progression of stone formation and kidney damage.

Current diagnostic alternatives remain limited, particularly when it comes to detecting cystine transport dysfunctions at the molecular level. Several practical bottlenecks have constrained the large-scale functional characterization of cystinuria-related variants. Radioisotope-based uptake assays using [35S]-l-cystine (Font et al., 2001) or [14C]-l-cystine (Mizoguchi et al., 2001; Lee et al., 2022) remain the established gold standard for transporter function, whereas the safety risks of radioisotope handling, the requirement for specialist licensed facilities, and the generation of radioactive waste jointly preclude routine or high-throughput use. Mass-spectrometry-based cystine quantification, while being sensitive, demands expensive instrumentation and technical expertise not readily available in most diagnostic laboratories (Servais et al., 2021). As a result, although the Human Gene Mutation Database (HGMD) (January 2025 version) lists over 278 pathogenic mutations in SLC3A1 and 182 in SLC7A9 (Stenson et al., 2003), only a small fraction have been functionally characterized, leaving a substantial proportion of identified variants classified as variants of uncertain significance (VUS) and limiting their clinical interpretability (Lee et al., 2022). These bottlenecks define a clear unmet need for sensitive, non-radioactive, scalable functional assays for cystine transporter variants.

Advances in molecular structural biology have created new avenues for understanding the pathophysiology of cystine stones. In particular, recent work on the SLC3A1/SLC7A9 complex structure has significantly improved our understanding of the molecular mechanisms underlying cystine transport (Wu et al., 2020; Yan et al., 2020; Lee et al., 2022). Additionally, advances in protein structure prediction, such as the use of AlphaFold, have provided unprecedented opportunities to model the structural consequences of genetic mutations in cystine transporter proteins (Zhang et al., 2024). These structural insights are valuable for understanding how mutations impact protein function and in turn cystine reabsorption in the kidneys.

To provide a rapid molecular pathological analysis technique of cystine stones, we present an integrated approach combining a fluorescence-based cystine transport assay with AlphaFold3-based structure prediction. We selected selenocystine as a functional surrogate for cystine on the following grounds: (i) Selenocystine is the direct selenium analogue of cystine, which differs only in the substitution of the disulfide bridge (–S–S–) with a diselenide bond (–Se–Se–); the two molecules share near-identical backbone geometry, charge distribution, and overall dimensions; (ii) the reduced form of cystine, selenocysteine, reacts with acrylate-containing fluorescent dyes ~100-fold faster due to the lower pKa and higher nucleophilicity of the selenol group, providing superior sensitivity; and (iii) the selenocystine/FOdA fluorescence method has established precedent in the cystine/glutamate antiporter SLC7A11 system (also known as xCT) (Shimomura et al., 2021). The fluorescence assay offers a sensitive and efficient method for detecting cystine transport activity, while AlphaFold enables the prediction of structural alterations in cystine transporter proteins caused by specific mutations. Our approach combines these two modalities—functional and structural—to bridge the gap between genetic mutation and

consequence at the protein level, with the goal of supporting more targeted diagnostic and therapeutic strategies for cystinuria.

2 Results

2.1 Selenocystine Transport by SLC3A1/SLC7A9

SLC3A1/SLC7A9 heterodimers are responsible for the reabsorption of cystine and basic amino acids in renal proximal tubules. On the basis of structural similarity among amino acids and a recent report that selenocystine can be transported by the SLC3A2/SLC7A11 complex (Shimomura et al., 2021), we hypothesized that selenocystine, the selenium analogue of cystine, could also serve as a substrate for SLC3A1/SLC7A9. To validate this hypothesis, we employed Atomic Absorption Spectroscopy (AAS) to quantify selenocystine uptake mediated by the SLC3A1/SLC7A9 heterodimer. As shown in Fig. 1a, selenium was detected exclusively in HEK293 cells co-expressing both SLC3A1 and SLC7A9. However, the time-consuming and complex operation of AAS limits its high-throughput application. We therefore applied a novel method to monitor SLC3A1/SLC7A9 transporting activity. The principle of the assay is to collect cell-incorporated selenocystine, reduce it to selenocysteine using tris(2-carboxyethyl)phosphine (TCEP), and allow the selenol group of selenocysteine to react with the acrylate moieties of Fluorescein O,O′-diacrylate (FOdA), in order to generate a fluorescent adduct with a specific excitation/emission peak (Fig. 1b).

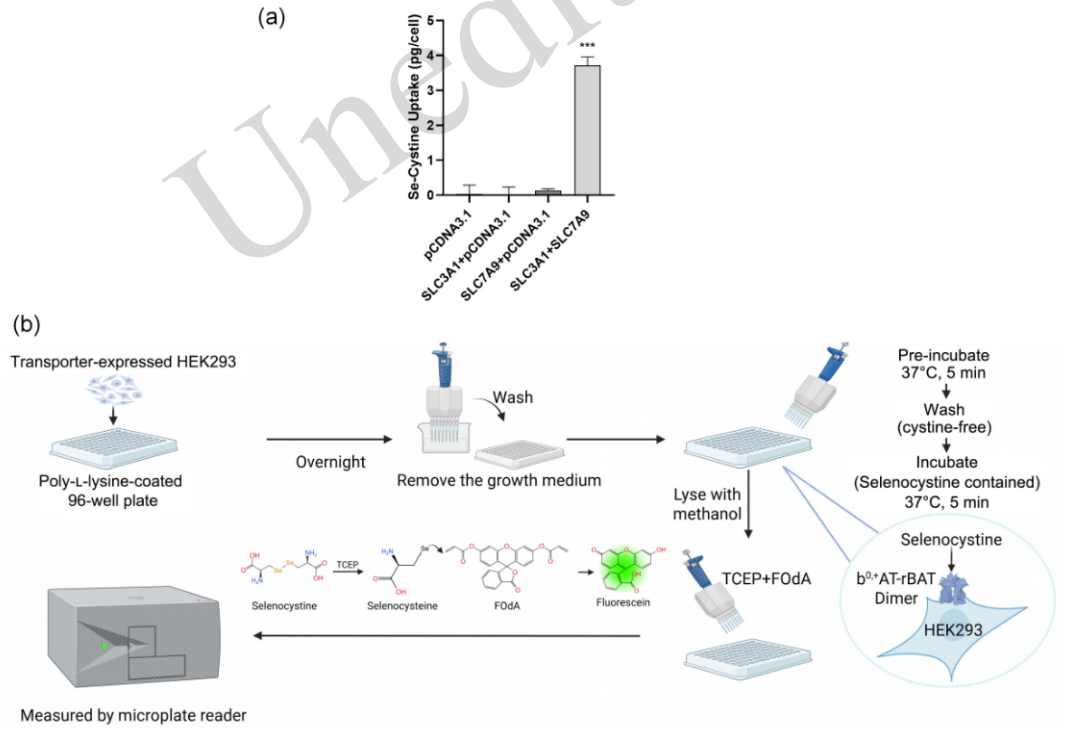

Fig. 1 SLC3A1/SLC7A9-dependent selenocystine uptake in HEK293 cells by Atomic Absorption Spectroscopy (AAS) and fluorescence uptake assay. (a) The cellular selenium content of HEK293 cells was quantified by AAS after 30-minute exposure to 200 μM selenocystine. Data represent functional uptake mediated by the SLC3A1/SLC7A9 heterodimer. The methodology details are provided in the Materials and Methods. The values are expressed as mean ± standard deviation (SD), n = 3. *** P<0.001. (b) Graphic Model of Selenocystine-Based Fluorescence Uptake Assay. TCEP, tris(2-carboxyethyl)phosphine; FOdA, Fluorescein O,O′-diacrylate; b0+AT-rBAT dimer, heterodimeric amino acid transporter composed of SLC7A9 (b0+AT) and SLC3A1 (rBAT); HEK293, human embryonic kidney 293 cells.

Due to the higher reducing activity of the selenol group, selenocystine is significantly more reactive in transforming the dye compared to cystine. As shown in Fig. 2a, the in vitro fluorescence signal was more than 100-fold stronger with selenocystine than that with cystine. We next tested the cellular uptake of selenocystine or cystine by HEK293 cells overexpressing SLC3A1/SLC7A9. As shown in Fig. 2b, the assay was sensitive enough to detect selenocystine incorporation at 25 μmol/L concentration incubation, while cystine incorporation was not detectable even at high concentrations (600 μmol/L). Additionally, the selenocystine incorporation was saturable and followed Michaelis-Menten kinetics with a Km of 156.3 ± 24.2 μmol/L and Vmax of 7.65 ± 0.45 fold of the base value. Fig. 2c shows that SLC3A1/SLC7A9 transport selenocystine in a time-dependent manner. These findings demonstrate the superior sensitivity of this assay for detecting selenocystine transport. To further validate that SLC3A1/SLC7A9 transporters are responsible for selenocystine transport, HEK293 cells were transfected with SLC3A1 or SLC7A9 alone or both. As shown in Fig. 2d, only HEK293 cells co-expressing SLC3A1 and SLC7A9 were able to detect the assay signal.

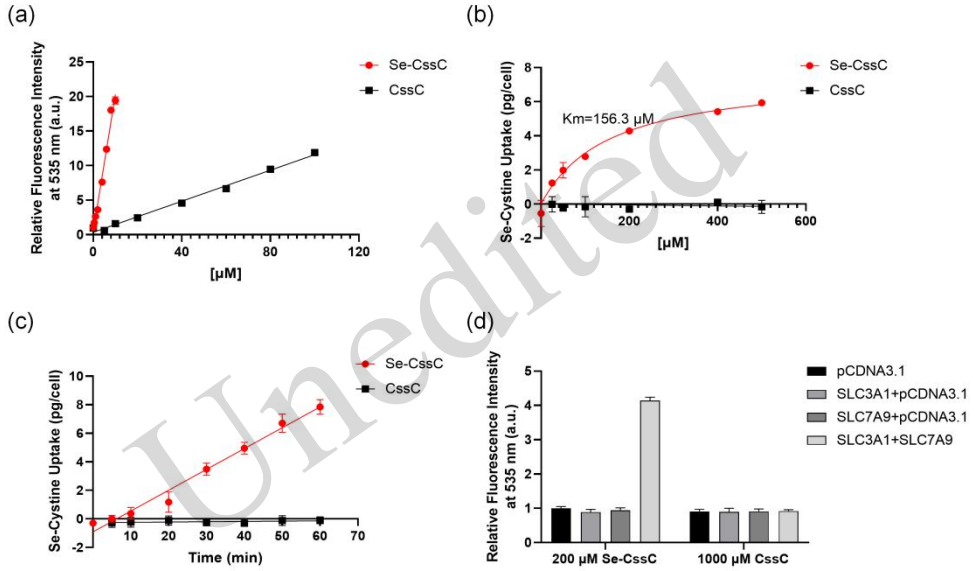

Fig. 2 Selenocystine can be taken up by SLC3A1/SLC7A9-expressing HEK293 cells. (a) Increasing concentrations of selenocystine (Se-CssC) and non-labeled cystine (CssC) in Hanks' buffer were reacted with FOdA substrate for 30 min at 37°C. Fluorescence signals generated by Se-CssC or CssC were measured using a multifunctional microplate reader. (b) Dose-dependent uptake of Se-CssC or CssC by SLC3A1/SLC7A9-expressing HEK293 cells. Cells were treated with increasing concentrations of Se-CssC or CssC for 30 minutes, and uptake was quantified using a standard curve. Selenocystine transport by SLC3A1/SLC7A9 was fitted to Michaelis-Menten equations, and Km and Vmax were determined by nonlinear regression using GraphPad Prism software. (c) Time-dependent uptake of Se-CssC or CssC by SLC3A1/SLC7A9-expressing HEK293 cells. Cells were incubated with 200 μmol/L Se-CssC or CssC for the indicated durations, and fluorescence intensity was measured to assess uptake over time. (d) HEK293 cells expressing the indicated transporter genes were treated with 200 μmol/L Se-CssC or 1,000 μmol/L CssC for 30 min. Fluorescence intensity was normalized to the control conditions. The values are expressed as mean ± SD, n = 3. P < 0.01.**

2.2 Transport Characteristics of Selenocystine and Cystine via SLC3A1/SLC7A9

Selenocystine has lower solubility in urine compared to cystine, while its significantly lower physiological concentration prevents crystallization under normal conditions. However, a dysfunction of SLC3A1/SLC7A9 transporters leads to impaired cystine reabsorption and cystine crystallization in the kidney. To assess whether cystine and selenocystine show comparable apparent affinity for SLC3A1/SLC7A9 transporters, we varied the ratio of cystine to selenocystine in the extracellular medium while keeping the total concentration constant. As shown in Fig. 3a, a cystine/selenocystine ratio of 1:1 reduced the fluorescent signal to ~50% of the signal observed with selenocystine alone, a 3:1 ratio reduced the signal to ~25%, and a 1:3 ratio retained ~75% of this

signal. The proportional change in fluorescent signal with varying cystine-to-selenocystine ratios indicates that cystine and selenocystine compete for the same transporter binding site with comparable apparent affinity, supporting the use of selenocystine as a reliable functional surrogate for cystine in this assay.

To further assess the selectivity of SLC3A1/SLC7A9 transporters, we utilized known basic amino acids substrates (lysine, arginine, and ornithine) to compete with selenocystine. As depicted in Fig. 3b, a 1:1 mixture of ornithine and selenocystine blocked over half of the transport signal, while a 3:1 mixture of ornithine and selenocystine blocked about 90% of the signal, indicating higher apparent affinity of the transporter for ornithine. Similarly, Figs. 3c and 3d illustrate that the selectivity for arginine and lysine is significantly greater than that for selenocystine. In contrast, neutral amino acids such as glycine, alanine and serine, and the acidic amino acids aspartate and glutamate, did not inhibit selenocystine transport (Figs. 3e and 3f). The tyrosine competition was constrained to a 3-fold competitor excess (600 μmol/L tyrosine vs. 200 μmol/L selenocystine) because of the aqueous solubility ceiling of tyrosine (~600–700 μmol/L at 37°C); no inhibition was observed, further supporting the conclusion that tyrosine is not a substrate. The overall hierarchy of substrate preference is consistent with previous studies based on isotopes (Bertran et al., 1992; Wells&Hediger, 1992; Chairoungdua et al., 1999), which highlights the reliability of the selenocystine-based fluorescence assay in evaluating transport selectivity.

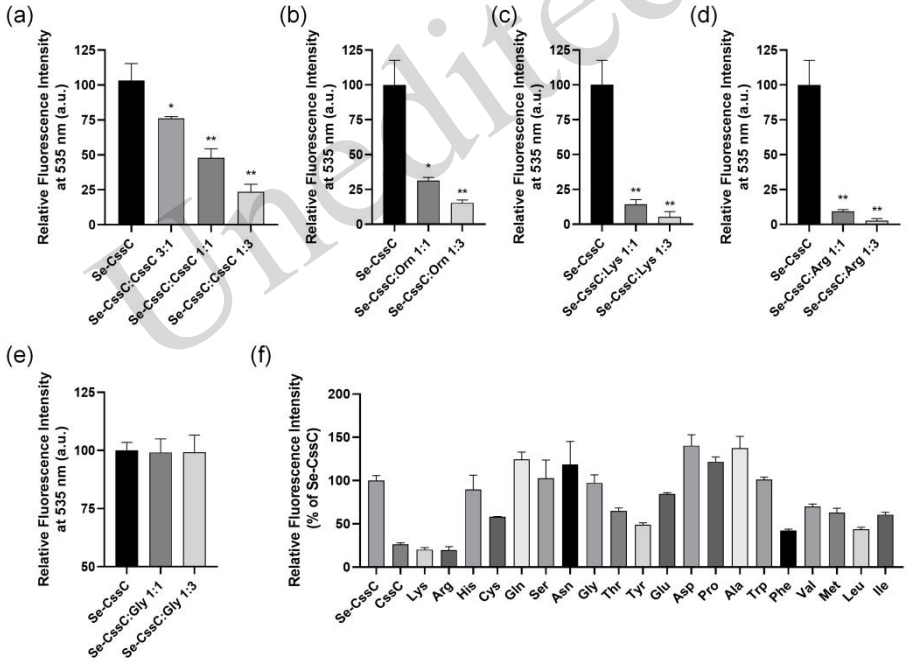

Fig. 3 Transport function and substrate selectivity of SLC3A1/SLC7A9. (a-e) Competitive inhibition of selenocystine transport by unlabeled amino acids. SLC3A1/SLC7A9-expressing HEK293 cells were treated with Se-CssC and competing amino acids (total concentration: 400 μmol/L) at ratios of 4:0 (control), 2:2, or 1:3 (selenocystine: competitor). Transport activity is expressed as a percentage relative to the control condition (Se-CssC only, 4:0 ratio). (a) Competition with cystine (CssC). (b) Competition with ornithine (Orn). (c) Competition with lysine (Lys). (d) Competition with arginine (Arg). (e) Competition with glycine (Gly). (f) Inhibition of selenocystine transport (200 μmol/L initial extracellular concentration) in competition assays containing 1 mmol/L unlabeled amino acid (as indicated, with the exception of tyrosine (Tyr), which was used at 600 μmol/L because of low solubility). Transport is displayed as percentage of no competing amino acid (only selenocystine). His, histidine; Cys, cysteine; Ser, serine; Asn, asparagine; Gln, glutamine; Thr, threonine; Tyr, tyrosine; Glu, glutamate; Asp, aspartate; Pro, proline; Ala, alanine; Trp, tryptophan; Phe, phenylalanine; Val, valine; Met, methionine; Leu, leucine; Ile, isoleucine. Data are presented as mean ± standard deviation (n≥3) from three independent experiments. Statistical significance was determined by comparison with the corresponding control group. *P < 0.05 and **P < 0.01.

To validate the assay against clinically annotated variants, we examined several clinically relevant missense variants of SLC7A9 and SLC3A1 previously characterized using radioisotope-based methods, selected according to pathogenic classification and population frequency in gnomAD and ClinVar. To enable transparent stratification, we classified variants as mild (residual transport activity > 60% of wild-type), moderate (20%–60% of wild-type), or severe (< 20% of wild-type), consistent with the qualitative classifications reported in the foundational radioisotope-based literature (Feliubadalo et al., 1999; Font et al., 2001).

SLC7A9 A182T (rs79389353; gnomAD frequency 0.004069, "Conflicting classifications of pathogenicity") and A70V (rs769448665; gnomAD frequency 0.000029, "Likely pathogenic") have previously been associated with mild functional impairment (Font et al., 2001; Reig et al., 2002). Consistent with those reports, both variants in this study showed only mild impairments in the selenocystine-based fluorescence assay (Figs. 4a and 4b). SLC7A9 G105R (rs121908480; frequency 0.000492) and R333W (rs121908484; frequency 0.000208), both classified as "Pathogenic/Likely pathogenic", have previously been associated with moderate-to-severe functional impairment (Font et al., 2001; Lee et al., 2022). Our assay results corroborated these findings, clearly showing moderate to severe transporter dysfunction (Figs. 4c and 4d). Furthermore, SLC7A9 P482L (rs146815072), SLC7A9 V170M (rs121908479), SLC7A9 A354T (rs939028046), and SLC3A1 M467T (rs121912691), all classified as "Pathogenic" or "Pathogenic/Likely pathogenic" have previously been reported as severe loss-of-function variants (Feliubadalo et al., 1999; Font et al., 2001; Reig et al., 2002; Shigeta et al., 2006; Lee et al., 2022); Consistent with those reports, all four showed near-complete loss of transport activity in our assay (Figs. 4e and 4f). The residual transport activities of all characterized variants are summarized in Table S2.

Collectively, these results confirm that the selenocystine-based fluorescence assay accurately and reliably captures the spectrum of transporter dysfunction caused by clinically significant mutations in SLC7A9 and SLC3A1, underlining its robustness and utility in functional diagnostics.

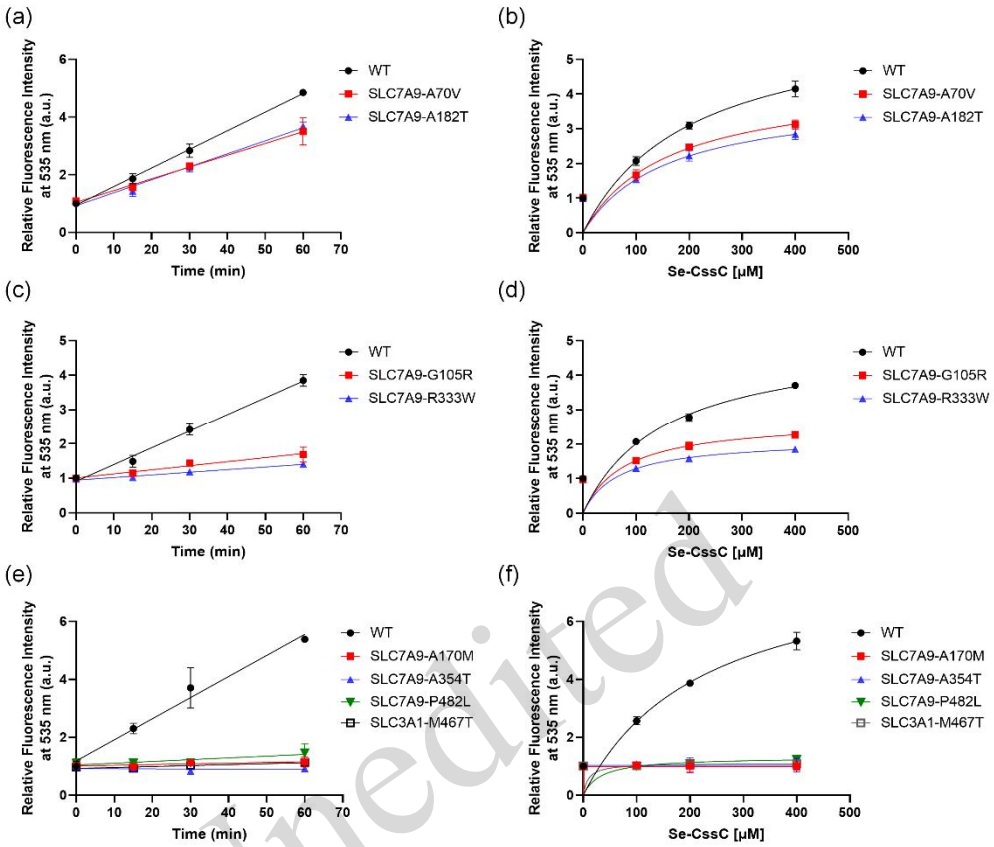

Fig. 4 Selenocystine Transport Capacity of Wild-Type and Clinically Reported Mutants of SLC7A9 and SLC3A1. HEK293 cells co-expressing wild-type (WT) *SLC3A1* with either wild-type *SLC7A9* or indicated mutants were treated with selenocystine. Transport activity (fluorescence intensity) is expressed as fold change relative to the base value (untreated control). (a) Time-dependent uptake of 200 μmol/L selenocystine by wild-type SLC7A9, SLC7A9-A70V, or SLC7A9-A182T. (b) Dose-dependent uptake of selenocystine (0–400 μmol/L, 30 min incubation) for wild-type SLC7A9, SLC7A9-A70V, or SLC7A9-A182T. (c–d) Time-dependent (c) and dose-dependent (d) uptake assays for wild-type SLC7A9, SLC7A9-G105R, or SLC7A9-R333W. (e–f) Time-dependent (f) and dose-dependent (f) uptake assays for wild-type SLC3A1/SLC7A9, SLC3A1-WT/SLC7A9-V170M, SLC3A1-WT/SLC7A9-A354T, SLC3A1-WT/SLC7A9-P482L, or SLC3A1-M467T/SLC7A9-WT. Data are presented as mean ± standard deviation (n=3).

2.3 Lack of Selenocystine Transport Capacity of SLC7A13 (AGT1)

An unsolved paradox in renal amino-acid transport is that SLC3A1 is highly expressed in the S3 segment of the proximal tubules, whereas SLC7A9 expression is highest in the S1 segment. Researchers have put forward the hypothesis that additional light- or heavy-chain partners exist for SLC3A1 and/or SLC7A9, and SLC7A13 (AGT1) has been proposed as the missing cystine transporter partner for SLC3A1 based on colocalization with SLC3A1 in the S3 segment and a report of cystine, aspartate and glutamate transport by purified AGT1–SLC3A1 reconstituted in proteoliposomes (Nagamori et al., 2016). Controversially, this proposal has faced scrutiny due to conflicting genetic evidence (Olschok et al., 2018).

We therefore used our assay to reexamine whether SLC7A13 mediates selenocystine transport in a cell-based context. Full dose–response curves (selenocystine, 0–600 μmol/L) were obtained for four transporter combinations expressed in HEK293 cells (Figs. 5a and 5b): SLC3A1/SLC7A13, SLC3A2/SLC7A13, SLC3A1/SLC7A11, and SLC3A2/SLC7A11. Neither SLC3A1/SLC7A13 nor SLC3A2/SLC7A13 produced a concentration-dependent fluorescence signal distinguishable from the untransfected blanks at any tested concentration. In contrast, the positive control SLC3A2/SLC7A11 displayed clear, saturable, and dose-dependent uptake, consistent with the known physiology of the xCT system, and SLC3A1/SLC7A11

produced no detectable signal, consistent with the established specificity of SLC7A11 for SLC3A2 as its obligate partner. These results indicate that in the present cell-based expression system, SLC7A13-containing complexes do not mediate detectable selenocystine transport.

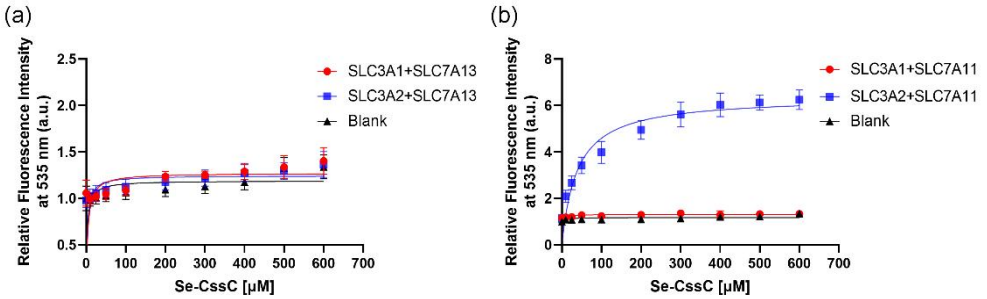

Fig. 5 Selenocystine Transport activity of other putative transporter complexes. (a) Dose-dependent uptake of selenocystine in HEK293 cells expressing *SLC3A1/SLC7A13* or *SLC3A2/SLC7A13*. (b) Dose-dependent uptake of selenocystine in HEK293 cells expressing *SLC3A1/SLC7A11* or *SLC3A2/SLC7A11*. Transfected cells were incubated with increasing concentrations of selenocystine (0, 10, 25, 50, 100, 200, 300, 400, 500, and 600 μmol/L) for 30 min. Untransfected cells (Blank) served as negative controls. Selenocystine uptake was determined by measuring fluorescence intensity at 535 nm using a multifunctional microplate reader. Transport activity is expressed as relative fluorescence intensity normalized to the untreated control. Values are expressed as mean ± SD (n=3). SLC7A11, solute carrier family 7 member 11; SLC7A13, solute carrier family 7 member 13.

2.4 Rapid Identification of AlphaFold-Predicted Structural Changes Causing Impairment

AlphaFold2 and AlphaFold3 have shown remarkable accuracy in predicting protein structures (Jumper et al., 2021; Abramson et al., 2024). When combined with small-molecule docking tools, these computational predictions provide a foundation for the mechanistic interpretation of cystinuria-related mutations. To assess whether AlphaFold3-predicted structural perturbations can rationalize the functional impairments measured in our assay, we compared the predicted structures of wild-type and mutant SLC7A9 alongside the corresponding selenocystine-uptake data, focusing on variants for which the prediction yielded a discrete, residue-level structural feature.

Two examples are given to directly illustrate the structure-function correlation. First, at position 482, the AlphaFold3 model places Pro482 at the cytoplasmic gate region of the transport channel, where its compact ring side chain leaves the substrate path unobstructed (Fig. 6a, left). The P482L substitution introduces a bulky leucine side chain that protrudes into the channel and sterically occludes the predicted substrate pathway (Fig. 6a, middle), whereas P482G leaves the channel essentially unobstructed (Fig. 6a, right). These predictions correlate directly with the measured transport activity: P482L retains only ~5% of wild-type activity, while P482G retains ~100% (Fig. 6b; Table S2). This pairing provides a structural rationale for the loss of function of P482L (Shigeta et al., 2006), which had not previously been mechanistically explained. Moreover, because a different substitution at the same residue (P482G) is predicted to leave the channel open and is functionally tolerated, it acts as an internal control that supports the specificity of the structural interpretation.

Second, the SLC7A9 A354T mutant, which retains <5% of wild-type transport activity (Figs. 4e and 4f; Table S2), does not directly contact the substrate channel in the AlphaFold3 model. Instead, the Thr354 side chain is predicted to disrupt local packing of the surrounding transmembrane helix and to propagate conformational changes to the distal residues Phe322 and Arg326, both of which reorient toward the transport channel (Fig. 6c). This predicted reorientation is consistent with the near-complete loss of transport activity observed experimentally and provides a mechanistic explanation for the dysfunction of a variant whose loss-of-function would not be obvious from the position of the mutated residue alone.

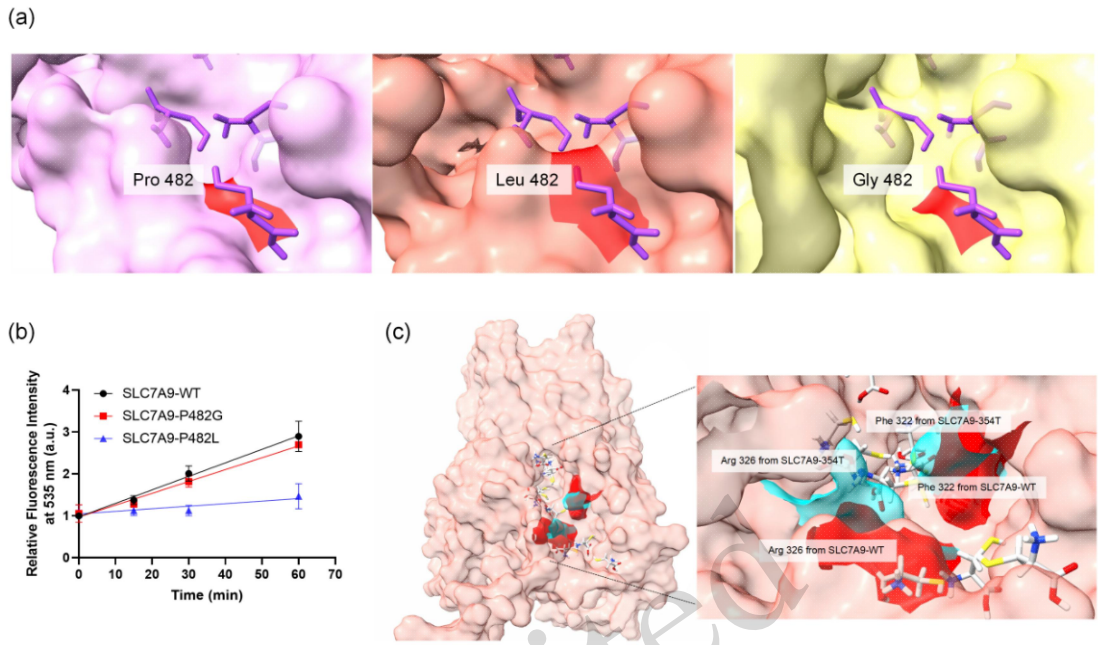

Fig. 6 Structure prediction and functional characterization of mutants of SLC7A9 by a selenocystine uptake assay. (a) Surface structural comparison of wild-type and mutant $b^{0,+}$AT at position 482. Left to right: Surface representations of wild-type $b^{0,+}$AT, P482L mutant, and P482G mutant. Residue 482 (red) highlights conformational changes induced by proline-to-leucine (P482L) or proline-to-glycine (P482G) substitutions. (b) HEK293 cells co-expressing wild-type *SLC3A1* with wild-type *SLC7A9*, *SLC7A9*-P482G, or *SLC7A9*-P482L were treated with 200 μmol/L selenocystine for the indicated duration. Transport activity (fluorescence intensity) is expressed as fold change relative to the base value (untreated control). Data are presented as mean ± SD (n = 3). (c) Structural perturbation of residues Phe322 and Arg326 induced by the A354T mutant of $b^{0,+}$AT. Surface representation of wild-type $b^{0,+}$AT (background, red) with residues Phe322 (right, red) and Arg326 (left, red). Structural rearrangements caused by the A354T mutation are shown in cyan. The mutation at position 354 (not displayed) disrupts local interactions, altering the conformation of distal residues 322 and 326.

Together, the explicit pairing of predicted structural perturbations with measured transport activities at two independent sites (P482 and A354) supports the value of combining AlphaFold3 modeling with the selenocystine fluorescence assay for variant interpretation in cystinuria. It should be noted that for the remaining variants in our panel (A70V, A182T, G105R, R333W, V170M, and SLC3A1 M467T), AlphaFold3 did not reveal a discrete structural feature comparable to the channel-occlusion or pocket-reorientation events seen at P482 and A354; rather than the over-interpretation of subtle model differences, we have limited the explicit structure-function pairings to cases where the prediction is both confidently supported (mean pLDDT > 80 in the affected region) and mechanistically interpretable. We further emphasize that AlphaFold3 produces computational models rather than experimental structures, hence the interpretations above will benefit from validation by Cryogenic Electron Microscopy (cryo-EM) or X-ray crystallography of selected mutants in future work.

3 Discussion

Traditional approaches for evaluating cystine transporter function, including radioisotope-based uptake assays and mass spectrometry-based cystine quantification, present significant limitations in clinical contexts. Although over 278 distinct pathogenic mutations have been reported in SLC3A1 and 182 in SLC7A9 (Stenson et al., 2003), only a small fraction have been functionally characterized. This gap is largely due to the impracticality of conventional assays for routine use: radioisotope methods carry safety risks and require

specialized facilities, while mass spectrometry demands expensive instrumentation and technical expertise not readily available in most laboratories (Servais et al., 2021). To address this need, our study introduces a non-radioactive fluorescence-based uptake assay using selenocystine as a cystine analog, enabling the sensitive, cost-effective, and scalable assessment of SLC3A1/SLC7A9 transporter function. In agreement with prior studies on the cystine/glutamate antiporter (Shimomura et al., 2021), we have confirmed that selenocystine closely mimics cystine in transport assays, supporting the validity of our fluorescence-based method for detecting cystine transport activity.

Our approach relies on standard microplate readers and non-hazardous reagents rather than radioactive substrates or capital-intensive equipment. This accessibility makes the assay well suited to systematic functional reclassification of the many SLC3A1 and SLC7A9 variants of uncertain significance currently catalogued in ClinVar and HGMD, providing the type of functional evidence increasingly valued in variant-interpretation frameworks. Notably, fluorometric detection methods are generally regarded as simple, rapid and highly sensitive, which is consistent with our findings (Kalaiyarasan et al., 2019).

A major finding of this study is the capacity of the proposed assay to evaluate the functional impact of clinically relevant variants in cystinuria. Specifically, variants previously associated with mild cystinuria phenotypes (e.g. SLC7A9 A70V and A182T) showed minimal transport impairment in our assay, whereas intermediate variants like SLC7A9 G105R and R333W led to moderate reductions in transport efficiency. Severe loss-of-function mutations including SLC7A9 P482L, V170M and A354T, and SLC3A1 M467T, exhibited near-complete loss of transport activity, aligning with the more severe clinical phenotype of patients (Font et al., 2001; Bartoccioni et al., 2008).

These results validate the proposed assay as a reliable tool for assessing transporter activity and demonstrate its capacity to stratify variants by functional severity. Such stratification may have future clinical relevance; however, translating these cell-based findings into the clinical prediction of disease severity and stone risk will require prospective validation in patient cohorts with known genotypes and phenotypes, including correlation with urinary cystine excretion and stone-recurrence rates. In addition, establishing standardized assay thresholds for mild, moderate and severe functional classifications will be a prerequisite for clinical implementation. To achieve this goal, validation in patient-derived samples (urinary exfoliated tubular cells or iPSC-derived renal organoids) offers a plausible route.

Our data also clarify the proposed role of SLC7A13 (AGT1) in renal cystine transport. In our cell-based system, SLC7A13-containing complexes showed no detectable selenocystine uptake, consistent with genetic evidence arguing against a major role for SLC7A13 in cystinuria (Olschok et al., 2018). The discrepancy with the previously reported proteoliposome-based activity may reflect differences between purified-protein reconstitution and intact mammalian cells, including post-translational modification, folding, and membrane context (Nagamori et al., 2016). Thus, our findings support SLC3A1/SLC7A9 as the principal cystine transporter complex relevant to cystinuria.

In addition to functional measurements, integrating structural predictions provide a mechanistic insight into how particular mutations cause transporter dysfunction. AlphaFold-based models can help explain, for example, how the SLC7A9 P482L mutation introduces a steric block in the transport pathway, correlating with the markedly reduced cystine uptake observed experimentally. Similarly, the A354T variant was found to disrupt transmembrane domain rotations, leading to transporter inactivation. These findings underline the potential of combining structural modeling with functional assays for the rapid and accurate characterization of cystine transport impairments.

As a limitation of this study, the structural analyses presented here rely on AlphaFold3-predicted models rather than experimentally determined structures. AlphaFold3 predictions, while locally reliable in high-pLDDT regions, do not capture dynamic conformational states, ligand-induced rearrangements, or the native membrane-lipid environment. Structural models were used to generate mechanistic hypotheses that were subsequently tested by the functional assay, providing an orthogonal line of evidence rather than relying on the predictions in isolation. Nevertheless, experimental validation by cryo-EM or X-ray crystallography of the

specific mutant complexes studied here, particularly P482L and A354T, would provide definitive structural confirmation and is identified as an important direction for future work.

In summary, our fluorescence-based selenocystine transport assay combining structural predictions provides a high-sensitivity, reliable tool for assessing cystine transporter function and identifying transport-deficient variants. Future studies should focus on validating its clinical applicability and integrating it into high-throughput screening platforms to facilitate cystinuria-related research and therapeutic development.

Materials and methods

Detailed methods are provided in the electronic supplementary materials of this paper.

Data availability statement

The data presented in this study are available from the corresponding author upon reasonable request.

Acknowledgments

This work was financially supported by Zhejiang Provincial Natural Science Foundation of China under Grant No. LMS25H160004, and Zhejiang Provincial Medical and Health Science and Technology Programs (2023KY650, 2021KY080). The authors acknowledge the support from the Scientific Research Center, Hangzhou Medical College.

Author contributions

Xiaobai HE took the responsibility for funding acquisition, investigation, methodology and data curation. Xinyi QIAN, Xiaoguang ZHENG, Hong ZHANG, Jinbang SHAO, and Qi RUAN participated in the investigation. Xiaopan CHEN provided Resource. Jianxin LYU and Leixiang YANG provided guidance for thesis and financial support. Linjie CHEN, took charge of the Conceptualization; Supervision; Writing-review & editing. All authors have read and approved the final manuscript.

Compliance with ethics guidelines

Xiaobai HE, Xinyi QIAN, Xiaoguang ZHENG, Hong ZHANG, Jinbang SHAO, Xiaopan CHEN, Qi RUAN, Jianxin LYU, Leixiang YANG and Linjie CHEN declare that they have no conflicts of interest.

This article does not contain any studies with human or animal subjects performed by any of the authors.

Declaration on the use of generative AI tools

During the preparation of this manuscript, the authors used ChatGPT to improve language and readability. The authors reviewed and edited all content and take full responsibility for the final publication.

References

Abramson J, Adler J, Dunger J, et al., 2024. Accurate structure prediction of biomolecular interactions with AlphaFold 3. *Nature*, 630(8016):493-500. http://doi.org/10.1038/s41586-024-07487-w

Bartoccioni P, Rius M, Zorzano A, et al., 2008. Distinct classes of trafficking rBAT mutants cause the type I cystinuria phenotype. *Hum Mol Genet*, 17(12):1845-1854. http://doi.org/10.1093/hmg/ddn080

Bertran J, Werner A, Moore ML, et al., 1992. Expression cloning of a cDNA from rabbit kidney cortex that induces a single transport system for cystine and dibasic and neutral amino acids. *Proc Natl Acad Sci U S A*, 89(12):5601-5605. http://doi.org/10.1073/pnas.89.12.5601

Chairoungdua A, Segawa H, Kim JY, et al., 1999. Identification of an amino acid transporter associated with the cystinuria-related type II membrane glycoprotein. *J Biol Chem*, 274(41):28845-28848. http://doi.org/10.1074/jbc.274.41.28845

Chillaron J, Font-Llitjos M, Fort J, et al., 2010. Pathophysiology and treatment of cystinuria. *Nature reviews Nephrology*, 6(7):424-434. http://doi.org/10.1038/nrneph.2010.69

Copelovitch L, 2012. Urolithiasis in children: medical approach. *Pediatric clinics of North America*, 59(4):881-896. http://doi.org/10.1016/j.pcl.2012.05.009

Feliubadalo L, Font M, Purroy J, et al., 1999. Non-type I cystinuria caused by mutations in SLC7A9, encoding a subunit (bo,+AT) of rBAT. *Nat Genet*, 23(1):52-57. http://doi.org/10.1038/12652

Font MA, Feliubadalo L, Estivill X, et al., 2001. Functional analysis of mutations in SLC7A9, and genotype-phenotype correlation in non-Type I cystinuria. *Hum Mol Genet*, 10(4):305-316. http://doi.org/10.1093/hmg/10.4.305

Jumper J, Evans R, Pritzel A, et al., 2021. Highly accurate protein structure prediction with AlphaFold. *Nature*, 596(7873):583-589. http://doi.org/10.1038/s41586-021-03819-2

Kalaiyarasan G, Hemlata C, Joseph J, 2019. Fluorescence Turn-On, Specific Detection of Cystine in Human Blood Plasma and Urine Samples by Nitrogen-Doped Carbon Quantum Dots. *ACS omega*, 4(1):1007-1014. http://doi.org/10.1021/acsomega.8b03187

Lee Y, Wiriyasermkul P, Kongpracha P, et al., 2022. Ca(2+)-mediated higher-order assembly of heterodimers in amino acid transport system b(0,+) biogenesis and cystinuria. *Nat Commun*, 13(1):2708. http://doi.org/10.1038/s41467-022-30293-9

Mizoguchi K, Cha SH, Chairoungdua A, et al., 2001. Human cystinuria-related transporter: localization and functional characterization. *Kidney Int*, 59(5):1821-1833. http://doi.org/10.1046/j.1523-1755.2001.0590051821.x

Nagamori S, Wiriyasermkul P, Guarch ME, et al., 2016. Novel cystine transporter in renal proximal tubule identified as a missing partner of cystinuria-related plasma membrane protein rBAT/SLC3A1. *Proc Natl Acad Sci U S A*, 113(3):775-780. http://doi.org/10.1073/pnas.1519959113

Olschok K, Vester U, Lahme S, et al., 2018. No evidence for point mutations in the novel renal cystine transporter AGT1/SLC7A13 contributing to the etiology of cystinuria. *BMC nephrology*, 19(1):278. http://doi.org/10.1186/s12882-018-1080-5

Reig N, Chillaron J, Bartoccioni P, et al., 2002. The light subunit of system b(o,+) is fully functional in the absence of the heavy subunit. *The EMBO journal*, 21(18):4906-4914. http://doi.org/10.1093/emboj/cdf500

Servais A, Thomas K, Dello Strologo L, et al., 2021. Cystinuria: clinical practice recommendation. *Kidney Int*, 99(1):48-58. http://doi.org/10.1016/j.kint.2020.06.035

Shigeta Y, Kanai Y, Chairoungdua A, et al., 2006. A novel missense mutation of SLC7A9 frequent in Japanese cystinuria cases affecting the C-terminus of the transporter. *Kidney Int*, 69(7):1198-1206. http://doi.org/10.1038/sj.ki.5000241

Shimomura T, Hirakawa N, Ohuchi Y, et al., 2021. Simple Fluorescence Assay for Cystine Uptake via the xCT in Cells Using Selenocystine and a Fluorescent Probe. *ACS sensors*, 6(6):2125-2128. http://doi.org/10.1021/acssensors.1c00496

Stenson PD, Ball EV, Mort M, et al., 2003. Human Gene Mutation Database (HGMD): 2003 update. *Human mutation*, 21(6):577-581. http://doi.org/10.1002/humu.10212

Thomas K, Wong K, Withington J, et al., 2014. Cystinuria-a urologist's perspective. *Nature reviews Urology*, 11(5):270-277. http://doi.org/10.1038/nrurol.2014.51

Wells RG, Hediger MA, 1992. Cloning of a rat kidney cDNA that stimulates dibasic and neutral amino acid transport and has sequence similarity to glucosidases. *Proc Natl Acad Sci U S A*, 89(12):5596-5600. http://doi.org/10.1073/pnas.89.12.5596

Wu D, Grund TN, Welsch S, et al., 2020. Structural basis for amino acid exchange by a human heteromeric amino acid transporter. *Proc Natl Acad Sci U S A*, 117(35):21281-21287. http://doi.org/10.1073/pnas.2008111117

Yan R, Li Y, Shi Y, et al., 2020. Cryo-EM structure of the human heteromeric amino acid transporter b(0,+)AT-rBAT. *Sci Adv*, 6(16):eaay6379. http://doi.org/10.1126/sciadv.aay6379

Zhang H, Lan J, Wang H, et al., 2024. AlphaFold2 in biomedical research: facilitating the development of diagnostic strategies for disease. *Front Mol Biosci*, 11:1414916.

http://doi.org/10.3389/fmolb.2024.1414916

Supplementary information
Materials and methods; Tables S1 and S2